https://doi.org/10.5194/essd-2024-334
Preprint. Discussion started: 22 August 2024

Seeing through the Sea with Satellites:
Reconstructing Ocean Subsurface Temperature and Salinity with Satellite Observations

Shizuo Liu and Shineng Hu
Nicholas School of the Environment, Duke University, Durham, NC, USA

Correspondence: Shineng Hu (shineng.hu@duke.edu)

Abstract. In-situ measurements of ocean temperature and salinity are critical to ocean-related studies but are limited in space and time. Satellite retrievals provide high-resolution, globally-covered sea surface temperature (SST), salinity (SSS) and cannot directly measure the subsurface information., and height (SSH), but are limited to the ocean surface and cannot directly measure the subsurface information. Here we design a physics-informed algorithm that can reconstruct the vertical distributions of upper ocean temperature and salinity based purely on satellite observations. The algorithm stresses the tight ocean surface-subsurface coupling and the co-variability of ocean temperature and salinity. It is firstly tested with climate model simulations and then validated with actual observations by Argo floats, moored buoys and multiple ocean reanalysis datasets. The resultant satellite-based upper ocean temperature and salinity dataset has a global coverage, a high spatial resolution, and resolves ocean thermohaline structure from surface to 400 m. This dataset complements existing ocean subsurface products as an independent satellite-based observational dataset. The success of our reconstruction algorithm highlights a pressing need to maintain and advance the satellite observations of SST, SSS, and SSH. The reconstructed ocean temperature and salinity dataset can be accessed at https://doi.org/10.5281/zenodo.13145129 (Liu, 2024) and be used by researchers to study mesoscale ocean phenomena, assess the ocean heat content in various sea areas and etc.

1 Introduction

Ocean temperature and salinity data are of immense importance for diverse climatic, environmental, ecological, and resource-related studies (Hughes et al., 2003; Cullum et al., 2016). The availability of high-resolution gridded ocean temperature and salinity data, covering the entire global ocean, thus holds the utmost significance for ocean and climate research (Abraham et al.,

https://doi.org/10.5194/essd-2024-334
Preprint. Discussion started: 22 August 2024

2013; Wunsch, 2015; Liang et al., 2021; Ponte et al., 2021). Before 2000, temperature and salinity data are primarily provided by ship-based profilers, e.g., Conductivity, Temperature, and Depth (CTD) or Expendable Bathythermograph (XBT), along major trade routes or scientific research vessels in target ocean regions. These ship-based measurements are sparce in space and time (Bagnell and DeVries, 2021), and sometimes only include the measurements of temperature, but not salinity (Zhang et al., 2023). Moored buoys (e.g., the TAO array) provide continuous in-situ measurements of temperature and salinity, but are only available at given sites and limited in space. Since 1999, the Argo program has been in operation, boosting a global network of approximately 4000 profiling buoys to date (Roemmich et al., 2019). It has the capability of long-term, automatic, real-time, and continuous acquisition of large-scale and deep data, and can provide ocean temperature and salinity from the surface to 2000 m (Riser et al., 2016; Wong et al., 2020). However, the irregular spatial distribution of Argo floats results in considerable uncertainties in temperature and salinity values, particularly in regions with low float density such as high latitudes and coastal areas (Roemmich et al., 2019). It will therefore be valuable to have an independent observational dataset to cross validate with other Argo-based products, especially when the latter diverge (Liu et al., 2022; Wong et al., 2023).

In recent decades, satellite-based ocean observations have been widely used (Loew et al., 2017; Vinogradova et al., 2019; Boutin et al., 2021; Fournier and Lee, 2021). Compared to Argo in-situ observations, satellite remote sensing data offers some advantages, including large-area synchronous measurement, high resolution, rapid acquisition speed, short update cycles, and abundant information (Boutin et al., 2021). However, satellite retrieved observations are limited to ocean surface properties such as temperature, salinity, and sea level, but not ocean subsurface temperature or salinity. This motivates us to explore whether it is possible to develop an algorithm capable of reconstructing ocean subsurface temperature and salinity using satellite observations. In the past, some attempts have been made to reconstruct subsurface temperature and salinity using diverse data sources, such as CTD data (Maes, 1999; Maes and Behringer, 2000), Argo data (Hosoda et al., 2008; Zhou et al., 2023), satellite data (Meng et al., 2021; Tian et al., 2022), or a combination of these (Guinehut et al., 2012; Stendardo et al., 2016). The methods employed can be categorized into two main groups. For traditional statistical methods, statistical relationships between surface and subsurface properties are firstly identified at the locations with available observations, and then subsurface ocean fields are reconstructed based on these correlations (Maes

https://doi.org/10.5194/essd-2024-334
Preprint. Discussion started: 22 August 2024

and Behringer, 2000; Fujii and Kamachi, 2003; Wang et al., 2012; Tang et al., 2022). These approaches typically do not incorporate satellite-observed surface salinity, which is critical to subsurface reconstruction as will be shown later, and have only been tested in selected ocean regions. Recently, machine learning-based methods have been proposed to reconstruct the ocean subsurface fields with satellite observations (Meng et al., 2021; Tian et al., 2022; Zhang et al., 2023). Although these advanced approaches have the capability to autonomously learn and generate fitting parameters without physics-based simplified assumptions, their complexity makes it elusive to provide coherent explanations for certain phenomena seen in the reconstructed data as part of the “black-box” constraint (Manucharyan et al., 2019; Tian et al., 2022).

In this study, we aim to develop a novel statistical approach to reconstruct ocean subsurface temperature and salinity fields using sea surface properties. Our algorithm is informed by three key ocean properties or assumptions. First, ocean temperature (T) and salinity (S) co-vary as they are simultaneously influenced by, for example, oceanic advection, warming-induced rainfall increase, etc (Troccoli and Haines, 1999; Kido et al., 2021). Second, ocean subsurface T and S variations are closely associated with ocean surface properties. Third, local vertical-temporal variations of ocean temperature and salinity can be decomposed into a set of orthogonal components. For each ocean grid, we firstly perform joint EOF analysis to $T(z,t)$ and $S(z,t)$ and identify a set of EOFs, $EOF\_T_i(Z)$ and $EOF\_S_i(Z)$, together with a principle component, $PC_i(t)$. We then regress $SSH(t)$ onto $PC_i(t)$ to obtain the associated EOF_SSH_i. With these known EOFs, the only information needed to reconstruct $T(z)$ and $S(z)$ is the principle component in front of each set of joint EOFs. To determine those coefficients, SST, SSS, and SSH will be used to minimize the joint cost function. Given the usage of three independent surface constraints, we will use the first three EOFs, which explains about 90% of the T-S variances on average (Fig. S1 in Supplement), to avoid an underdetermined system. Accordingly, we propose the algorithm as is illustrated in Fig. 1 (also see Data and Methods). The example in the flowchart is for the grid located at 8.5°S, 150.5°W in January 2016, at the peak of a strong El Nino event, with the total explained variance of the first three EOFs at this gird reaching nearly 90%.

https://doi.org/10.5194/essd-2024-334
Preprint. Discussion started: 22 August 2024

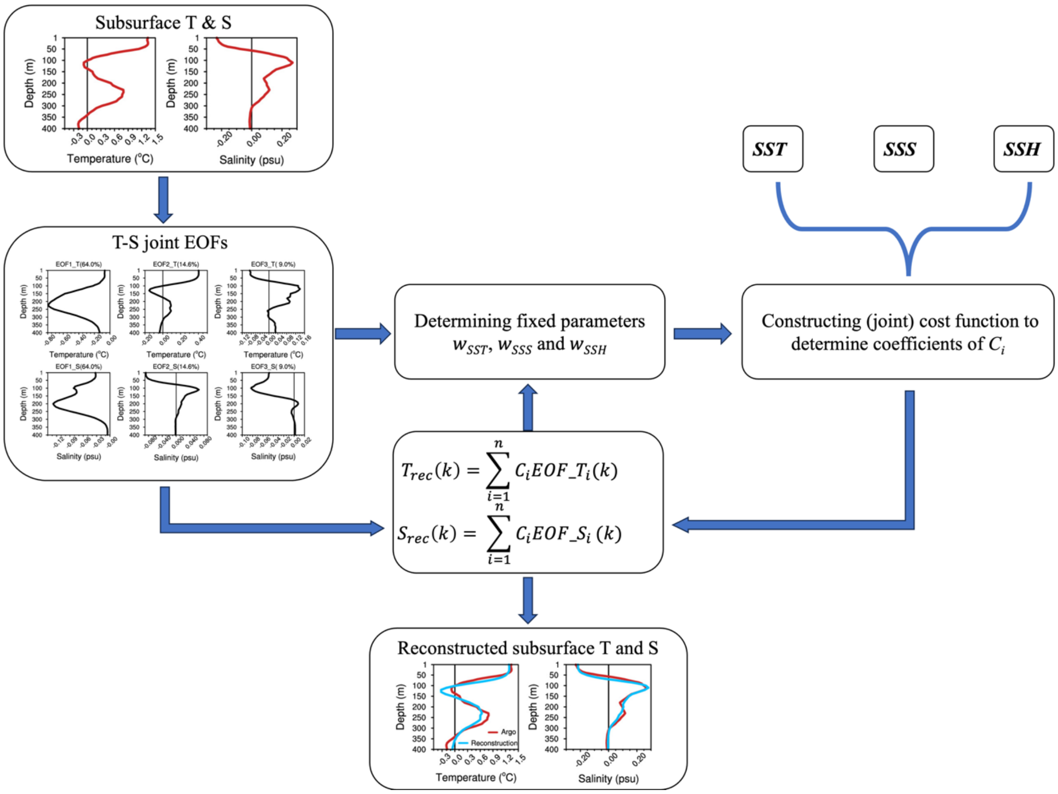

Figure 1. Flowchart of the algorithm proposed to reconstruct subsurface temperature and salinity with satellite observations. Argo profiles at 8.5°S, 150.5°W in January 2016 are shown as an example for the purpose of illustration. The black curves correspond to the first three T-S joint EOF modes at this ocean grid. The first row is EOF_T and the second row is EOF_S. The explained variances of the first three EOFs are 64.0%, 14.6% and 9.0%, respectively. The actual temperature and salinity profiles (red curves) do not look alike any of the EOFs (black curves), and our algorithm is able to accurately capture them based purely on the ocean surface information (*cf.* blue and red curves).

2 Data and Methods

2.1 Satellite-based observational datasets

Multiple satellite-based observational datasets are used. The sea surface temperature (SST) is from the National Oceanic and Atmospheric Administration (NOAA) 0.25° Daily Optimum Interpolation Sea Surface Temperature (OISST) version 2.1 (Huang et al., 2021), covering the period from September 1, 1981 to present. The sea surface salinity (SSS) is from Multi-Mission Optimally Interpolated Sea Surface Salinity (OISSS) Global Monthly Dataset V1 (Melnichenko et

https://doi.org/10.5194/essd-2024-334
Preprint. Discussion started: 22 August 2024

al., 2021). It has a 0.25° spatial and monthly temporal grid, covering the period from September 1, 2011 to December 31, 2020. This dataset uses three satellite missions: the Aquarius/SAC-D, Soil Moisture Active Passive (SMAP) and Soil Moisture and Ocean Salinity (SMOS). The sea surface height (SSH) is from MEaSUREs Gridded Sea Surface Height Anomalies Version 2205 (Fournier et al., 2022). It has a 0.17° spatial and 5-day temporal grid, covering the period from October 1, 1992 to December 31, 2022. This dataset is derived from the along-track SSHA data of TOPEX/Poseidon, Jason-1, Jason-2, Jason-3, Jason-CS (Sentinel-6).

2.2 In-situ observational datasets

In addition to the satellite-based datasets, in-situ measurements of ocean subsurface temperature and salinity, archived by the Argo floats (Gaillard et al., 2016) will be used. The Argo dataset used in this study has a 0.5° spatial and monthly temporal grid, covering the period from January 1, 2002 to December 31, 2020. This dataset is interpolated on 187 standard depth levels between 0-2000 m depth.

2.3 Ocean assimilation products

For comparison, monthly temperature and salinity from four ocean assimilation datasets are used in this study, including ORAS5, SODA3, IAP, and ECCO4r4 as introduced below. (1) The European Centre for Medium-Range Weather Forecasts (ECMWF) Ocean Reanalysis System 5 (ORAS5) (Zuo et al., 2019) is a global ocean and sea ice reanalysis monthly dataset that assimilated various observational data in an ocean model at a resolution of 0.25° × 0.25° and has 75 layers from 0.5 m at the top to 5902 m at the bottom. (2) The Simple Ocean Data Assimilation project version 3 (SODA3) (Carton et al., 2018), created by the University of Maryland, is constructed upon the Modular Ocean Model v5 ocean component of the Geophysical Fluid Dynamics Laboratory CM2.5 coupled model. It has an enhanced horizontal resolution of 0.25°, with 50 layers spanning from 5 m to 5395 m. (3) The Institute of Atmospheric Physics ocean data (IAP) (Cheng et al., 2017) provides global ocean coverage at a horizontal resolution of 1° × 1° across 41 vertical levels spanning from 1 to 2000 m. This dataset integrates in situ salinity profiles with coupled model simulations to generate an objective analysis using the ensemble optimal interpolation approach. (4) NASA's Estimating the Circulation and Climate of the Ocean project version 4, Release 4 (ECCO4r4) (ECCO Consortium et al., 2021), which is based on the

https://doi.org/10.5194/essd-2024-334
Preprint. Discussion started: 22 August 2024

Massachusetts Institute of Technology general circulation model (MITgcm) with a prognostic dynamic and thermodynamic sea ice model. It has 50 vertical levels spanning from 5 m to 5906 m and a horizontal resolution of 0.5° × 0.5°.

2.4 TAO/TRITON Moored Buoys array dataset

In-situ buoy measurements of temperature and salinity are used for further validation. The Tropical Atmosphere Ocean (TAO)/TRIangle Trans Ocean buoy Network (TRITON) array (TAO/TRITON) (Hayes et al., 1991) were built in the 1980s-1990s and provides since then continuously temperature and salinity measurements at a fixed location with high temporal resolution but a low vertical resolution (~20 m, covering 1 m to 200 m in most sites). It spans the tropical Pacific Ocean from 95°W in the eastern Pacific to 137°E in the western Pacific between 9°N and 8°S. In this study, we analyze temperature and salinity data from a single site, chosen for its complete time period coverage (2012-2020), selected from a limited number of sites that have a sufficiently long record for validation.

2.5 Community Earth System Model2 (CESM2) outputs

To evaluate the performance of the statistical model in this study, we use a list of output variables (SST, SSS, SSH, ocean subsurface temperature and salinity) for CESM2 historical run (Danabasoglu et al., 2020) to verify. We use the monthly data from 'r1i1p1f1' member with a nominal resolution of 100 km spatial and monthly temporal grid, covering from January 1, 1850 to December 31, 2014. This dataset is interpolated on 60 standard depth levels between 0-2000 m depth.

2.6 The reconstruction algorithm

Previous study found that the climatological temperature and salinity data had a close relationship (Stommel, 1947), known as the temperature-salinity (T-S) relationship, but this relationship undergoes variations over time and across different oceans. Maes and Behringer (2000) estimated the salinity profiles using the T-S relationship combined with the empirical orthogonal functions (EOFs) method via a weighted least squares procedure. While this approach attained a certain level of success within particular oceanic regions, it is unable to produce a high-resolution global dataset with CTD datasets that are limited in space. Besides, their methodology relies on

https://doi.org/10.5194/essd-2024-334
Preprint. Discussion started: 22 August 2024

both surface and subsurface data for reconstructing subsurface salinity, indicating limited applicability. Informed by these studies, in this study, we develop a statistical approach for reconstructing the subsurface temperature and salinity using high-resolution satellite ocean surface observations (Fig. 1).

First, the vertical EOFs of the combined subsurface T and S variability are used to present their vertical structures (Maes, 1999; Maes and Behringer, 2000). For each gird, we can define the vector:

$$X=[T(1)/\sigma_{T(1)}, T(2)/\sigma_{T(1)}, \cdots, T(N)/\sigma_{T(1)}, S(1)/\sigma_{S(1)}, S(2)/\sigma_{S(1)}, \cdots, S(N)/\sigma_{S(1)}] \quad (1)$$

where N is a constant corresponding the index when depth=400m. $T_1, \cdots, T_N, S_1, \cdots, S_N$ is defined as the departure from the climatology. To jointly account for the temperature and salinity variabilities, we normalize them by their own standard deviation at the surface layer. After performing the joint EOF analysis, we obtain several eigenmodes with real eigenvalues that are orthogonal to each other. Next, we regress the subsurface temperature and salinity anomalies onto each normalized eigenvector to obtain the distinct EOF modes of T (called EOF_T) and S (called EOF_S), respectively. We can further derive EOF_SSH_i by regressing the satellite-observed SSH onto the normalized eigenvector of the ith mode found in the T-S joint EOF analysis. It is important to note that the joint EOF analysis described above only needs to be done once with the existing data, and will then be used for all future reconstructions. In other words, subsurface reconstructions will only need new satellite observations of ocean surface properties and the previously computed, unchanged EOF basis from the joint EOF analysis.

To do the subsurface reconstruction, we assume the variations in the subsurface temperature and salinity anomalies can be expressed as a set of T-S joint EOFs by a linear combination of the dominant modes:

$$T_{rec}(k) = \sum_{i=1}^{n} C_i EOF\_T_i(k), \ S_{rec}(k) = \sum_{i=1}^{n} C_i EOF\_S_i(k) \quad (2)$$

where k represents vertical levels from surface down to 400 m, n is the number of vertical modes. C_i is the coefficient of each mode. To clarify, $EOF\_T_i(k)$ and $EOF\_S_i(k)$ are the joint EOFs calculated from monthly subsurface temperature and salinity anomalies. $T_{rec}(k)$ and $S_{rec}(k)$ are the vertical profiles of temperature and salinity anomalies to be reconstructed.

After these EOFs are computed, the only information needed to reconstruct $T_{rec}(k)$ and $S_{rec}(k)$ are the values of C_i's at each month. To determine those coefficients, SST, SSS, and SSH will be employed to minimize the (joint) cost function below:

https://doi.org/10.5194/essd-2024-334
Preprint. Discussion started: 22 August 2024

$$J = w_{SST}\left[\sum_{i=1}^{n} C_i EOF\_T_i(1) - SST_{obs}\right]^2/\sigma_{SST}^2 + w_{SSS}\left[\sum_{i=1}^{n} C_i EOF\_S_i(1) - SSS_{obs}\right]^2/\sigma_{SSS}^2 + w_{SSH}\left[\sum_{i=1}^{n} C_i EOF\_SSH_i - SSH_{obs}\right]^2/\sigma_{SSH}^2 \quad (3)$$

σ_{SST} , σ_{SSS} and σ_{SSH} represent the standard deviation of SST, SSS and SSH respectively. w_{SST}, w_{SSS} and w_{SSH} are constants which need to be given appropriate values. Notably, while SSH is linked to SSS and SST, our research finds that the introduction of SSH enhances the reconstruction performance. This cost function is a linear combination of the least-square difference between the actual surface and reconstructed surface variables.

To determine the three weighting parameters (w_{SST}, w_{SSS} and w_{SSH}) above that yield the best performance, we use the following formula.

$$J_t = \sum_{t=1}^{M}\sum_{k=1}^{N}[T_{rec}(k,t) - T_{obs}(k,t)]^2/\sigma_{T(1)}^2 + \sum_{t=1}^{M}\sum_{k=1}^{N}[S_{rec}(k,t) - S_{obs}(k,t)]^2/\sigma_{S(1)}^2 \quad (4)$$

where t represents the time and M is the total number of all months. For each set of subjective weighting parameters (w_{SST}, w_{SSS} and w_{SSH}), we calculate the corresponding J_t. Next, these values are used in Eq. (4) to compute the cumulative errors in temperature and salinity across all subsurface layers throughout the entire time period. This process helps identify the optimal weighting parameters for minimizing these errors. Globally averaged, the relative magnitude of the three weighting parameters (w_{SST}, w_{SSS} and w_{SSH}) is about 1:1.6:1.1. It highlights the fact that the information of sea surface salinity is critical to the performance of subsurface reconstruction. When w_{SST}, w_{SSS} and w_{SSH} are determined, we can incorporate them into Eq. (3) and solve for C_i's. With these values, we could reconstruct $T_{rec}(k)$ and $S_{rec}(k)$. It is worth noting that w_{SST}, w_{SSS} and w_{SSH} do not change with time but are fixed constants and that C_i's may change by time. In this approach, we limit our consideration to the first three EOFs when solving for C_i's, as there are only three input quantities (SST, SSS and SSH).

The joint EOF may differ by space, motivating us to apply the aforementioned procedures separately to obtain distinct coefficients for each ocean grid. When the C_i of each grid point is determined, we use the EOFs of each grid to reconstruct temperature and salinity anomalies individually. When conducting EOF analysis, we do not differentiate the anomaly fields among different seasons. Instead, we perform EOF analysis on the entire time period to ensure a sufficiently long-time dimension for the data.

The reconstruction algorithm has been firstly trained using the 165-year (1850-2014) data from the CESM2 historical runs to evaluate its performance. Climate model simulations like

https://doi.org/10.5194/essd-2024-334
Preprint. Discussion started: 22 August 2024

CESM2 have self-consistent surface and subsurface variables. The reconstruction results with the values of w_{SST}, w_{SSS} and w_{SSH} from the entire simulation period (1850-2014) are presented in the main text, and these results do not change much when a shorter period is used. For observations, the requirement for satellite and in-situ measurements lead to a short overlapping period of 2012-2020. We will train the statistical model in a certain period (i.e., 2012-2019) and validate with the rest (i.e., 2020), with a total of 9 rounds of training and verification being performed. Based on our sensitivity test, the results remain almost the same as the case with the entire period of 2012-2020 being used for training.

3 Results

3.1 Testing the performance of the algorithm with climate model output

Before being applied to observations, our reconstruction algorithm is firstly tested with a 165-year (1850-2014) historical simulation of a climate model, CESM2, that has self-consistent surface and subsurface variables. As an example, we first compare the spatial distribution of the CESM2 actual values and reconstructions for January 1860 at the peak of a strong El Niño. Our algorithm successfully reconstructs upper ocean temperature and salinity anomalies in the world ocean, including the tropical eastern Pacific warming, the western Pacific freshening, and the concurrent temperature and salinity changes in the world ocean (Fig. 2). Some mismatches are discussed below. For example, temperature mismatches are found around the Southern Ocean and the maritime continent, and salinity mismatches are found near the Maritime Continent and the Somali Basin. Since our study only uses the first three EOFs, this approach may result in errors particularly in regions where the dominant modes are not readily apparent or their contributions are limited (Troccoli and Haines 1999; Kido et al. 2021).

https://doi.org/10.5194/essd-2024-334
Preprint. Discussion started: 22 August 2024

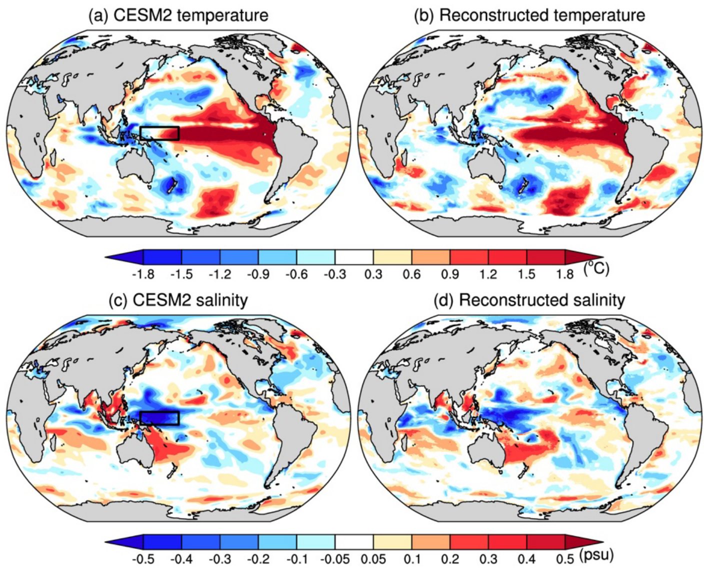

Figure 2. Comparisons of the global spatial distribution of CESM2 actual (left column) and reconstructed (right column) ocean subsurface temperature (a, b) and salinity (c, d) anomalies for the average of 1-100 m in January 1860. The black boxes in (a) and (c) correspond to the tropical western Pacific region ($140^oE - 180^o, 5^oS - 5^oN$) used for Fig. 3 and 4.

We next use the equatorial western Pacific (black boxes in Fig. 2a and c), which has abundant subsurface temperature variations with little surface signature, as an example to further illustrate the performance of our algorithm. Figure 3 shows the Time-Depth Hovmöller plots of the monthly CESM2 actual and reconstructed values in the tropical western Pacific region, spanning from 2010 to 2014. The reconstruction accurately captures the vertical structure of both temperature and salinity variations for the entire period. The annual average time series of the CESM2 actual data also consistently aligns well with the reconstructions across various depths in the tropical western Pacific region (Fig. 4), spanning from 1850 to 2014. In general, the mismatches between actual and reconstructed temperature and salinity, particularly below 100 m, can result from that only 3 EOFs are used in our algorithm or that subsurface salinity and temperature variations do not always pertain surface signals. Despite these limitations, our reconstruction algorithm can reasonably reproduce the spatial, vertical, and temporal characteristics of temperature and salinity variations in CESM2.

https://doi.org/10.5194/essd-2024-334
Preprint. Discussion started: 22 August 2024

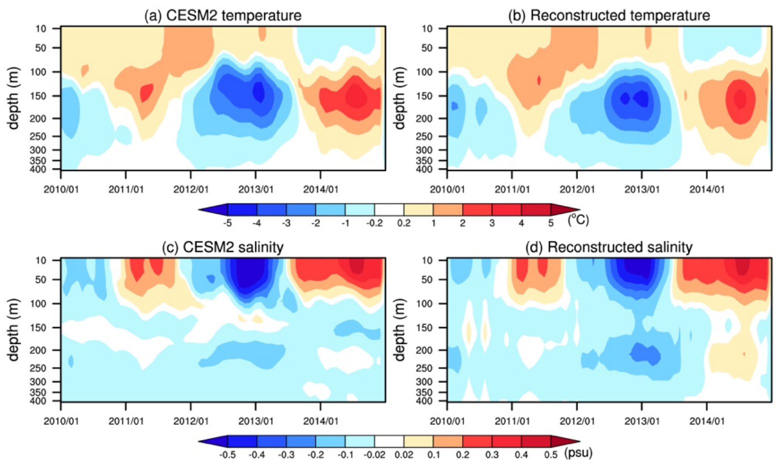

Figure 3. Comparisons of the Time-Depth Hovmöller plots of CESM2 actual (left column) and reconstructed (right column) ocean subsurface temperature (a, b) and salinity (c, d) anomalies over the tropical western Pacific region ($140^oE - 180^o, 5^oS - 5^oN$) during 2010-2014.

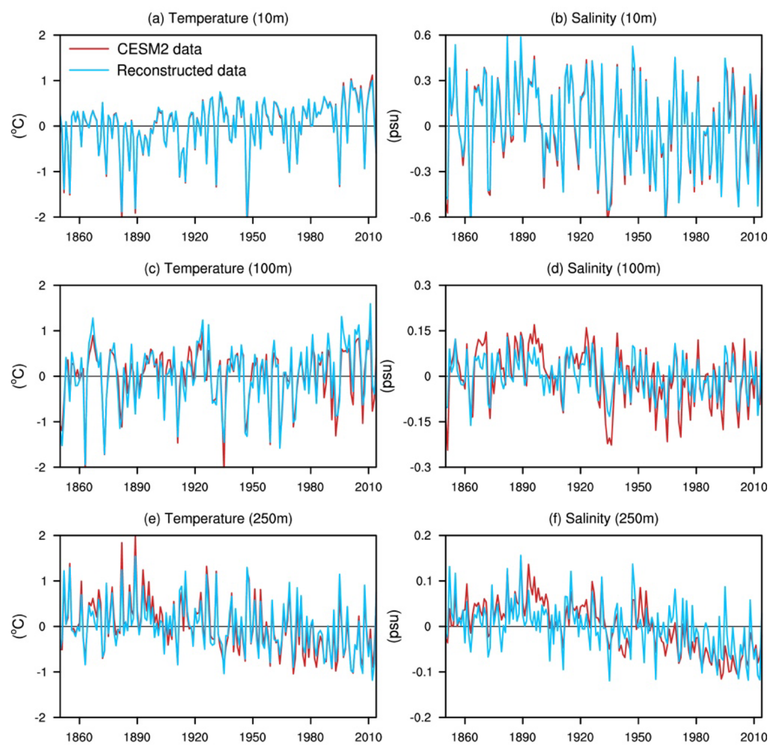

Figure 4. Comparisons of the time series of CESM2 actual (red line) and reconstructed (blue line) contrast time series for ocean subsurface temperature (left column) and salinity (right column) anomalies at 10 m (a, b), 100 m (c, d) and 250 m (e, f) depths for the tropical western Pacific region ($140^oE - 180^o, 5^oS - 5^oN$) during 1850-2014.

https://doi.org/10.5194/essd-2024-334
Preprint. Discussion started: 22 August 2024

3.2 Satellite-based ocean subsurface temperature and salinity reconstruction

The success of our algorithm in reconstructing the CESM2 subsurface fields leads us to further apply it to observations (see Data and Methods for detailed data description). At each ocean grid, historical Argo in-situ data are used to obtain the T-S joint EOFs, done once for all, and satellite measurements of SST, SSS, and SSH are then used as surface constraints to reconstruct the subsurface fields. Firstly, we assess the global pattern of our reconstructed fields averaged within the upper 100 m for January 2016 at the peak of an extreme El Niño as an example (Fig. 5). Using other time snapshots will yield similar conclusions. The large-scale pattern of the reconstructed temperature field closely match those of Argo in-situ data: including a considerable warming in the tropical eastern Pacific, a cooling in the tropical western Pacific, and a weak warming in the tropical Indian Ocean. The main features in the salinity field has also been well reproduced, including a negative anomaly in the tropical central-eastern Pacific, a positive anomaly in the tropical western Pacific, and a negative anomaly tropical eastern Indian Ocean. It is worth noting that the two El Niño events in Fig. 2 and 5 exhibit different spatial structures of temperature/salinity anomalies, particularly in the western Pacific region, which highlights that the reconstruction can well capture the diversity of El Niño events. Overall, the reconstructed and the original Argo fields for January 2016 have a global spatial correlation of 0.88 (Fig. 5a-c) for temperature and 0.86 for salinity (Fig. 5d-f) at a 2°x2° spatial resolution. If a finer resolution (e.g., 0.25°x0.25°) is used, the spatial correlations will slightly drop, but the reconstructed fields now contain fine-scale features that are absent in Argo datasets (Fig. S2 in Supplement) because of the usage of high-resolution satellite observations.

https://doi.org/10.5194/essd-2024-334
Preprint. Discussion started: 22 August 2024

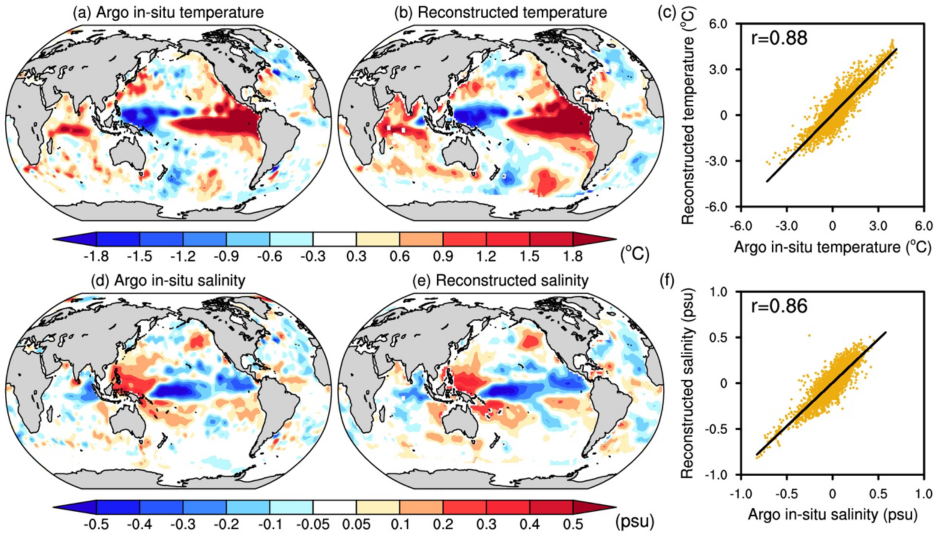

Figure 5. Comparisons on the global spatial distribution of Argo in-situ (left column) and reconstructed (middle column) ocean subsurface temperature (a, b) and salinity (d, e) anomalies for the average of 1-100 m in January 2016. Scatter plots (right column) of Argo in-situ versus reconstructed temperature anomalies (c) and salinity anomalies (f) for all the global grids in January 2016. The correlation r between Argo in-situ data and reconstruction is shown in the left-upper side of each panel. Both Argo in-situ and reconstructed datasets are interpolated to a 2° x 2° resolution in this figure, and the high-resolution version is shown in Fig. S2 in Supplement.

To further assess our algorithm, we select three representative ocean regions that have distinctive vertical structures of T-S variations, including the equatorial western Pacific, the equatorial eastern Pacific and the North Pacific Blob region (Fig. 6). In the equatorial eastern Pacific, its temperature variability peaks at 70 m and has a considerable surface signature as manifested by El Niño. The equatorial western Pacific has large subsurface ocean heat content variations, critical for El Niño preconditioning, but its surface temperature variability is rather weak. For both regions, salinity variability peaks at the surface, decays with depth, and increases again until reaching another local peak (Maes, 1999), and such intricate vertical structures presumably pose a challenge in reconstructing subsurface salinity. In the North Pacific Blob region, both temperature and salinity variabilities stay roughly uniform in the upper 100 m and decrease with depth below that. Meanwhile, these results indicate the significant differences in temperature and salinity changes across various ocean regions, highlighting the necessity of evaluating the performance of the reconstruction algorithm in diverse ocean regions.

https://doi.org/10.5194/essd-2024-334
Preprint. Discussion started: 22 August 2024

Open Access Earth System Science Data Discussions

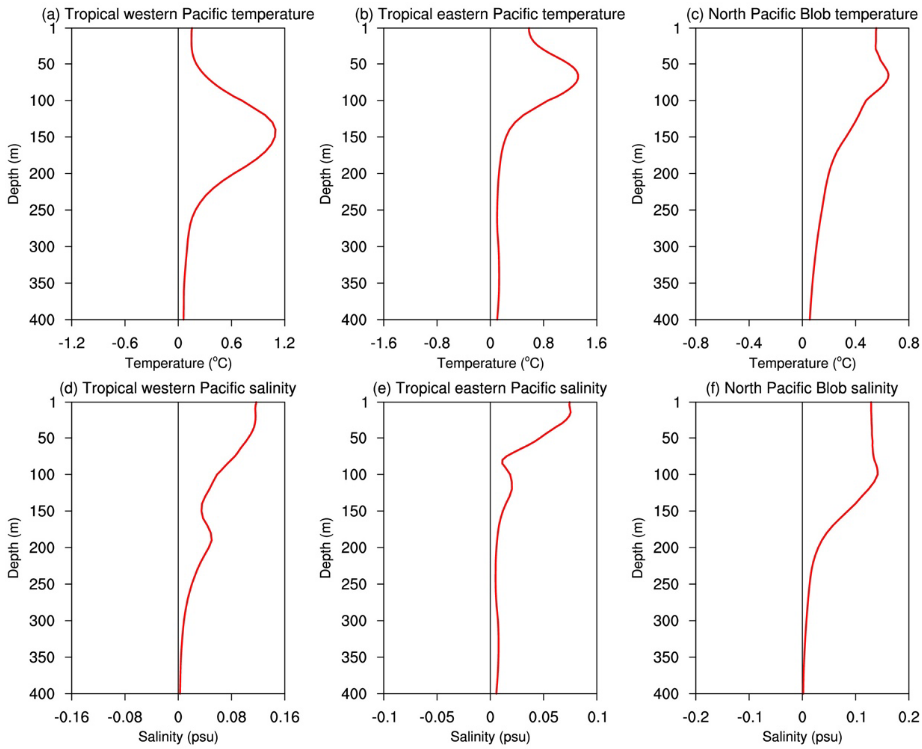

Figure 6. The vertical profile of the standard deviation in annual average temperature (a, b, c) and salinity (d, e, f) anomalies across the three regions tropical western Pacific ($140^oE - 180^o, 5^oS - 5^oN$), tropical eastern Pacific ($130^oW - 95^oW, 5^oS - 5^oN$), and North Pacific Blob region ($150^oW - 130^oW, 35^oN - 48^oN$).

The Time-Depth Hovmöller plots of the Argo in-situ data are compared with reconstructed temperature and salinity anomalies in the aforementioned three regions (Fig. 7 and 8). For the equatorial western Pacific, strong subsurface temperature anomalies can be reconstructed even when surface temperature anomalies almost vanish, and the double peaks of the same sign in the vertical structure of salinity anomalies can also be well captured. For the equatorial eastern Pacific, surface and subsurface temperature anomalies tend to show the same sign, while salinity anomalies exhibit a vertical dipole structure, both successfully captured by our reconstruction. For the North Pacific Blob region, the two-year marine heatwave event in 2014-15 and its downward propagation can be reconstructed, but the salinity reconstruction seems to be less satisfactory.

https://doi.org/10.5194/essd-2024-334
Preprint. Discussion started: 22 August 2024

Open Access Earth System Science Data Discussions

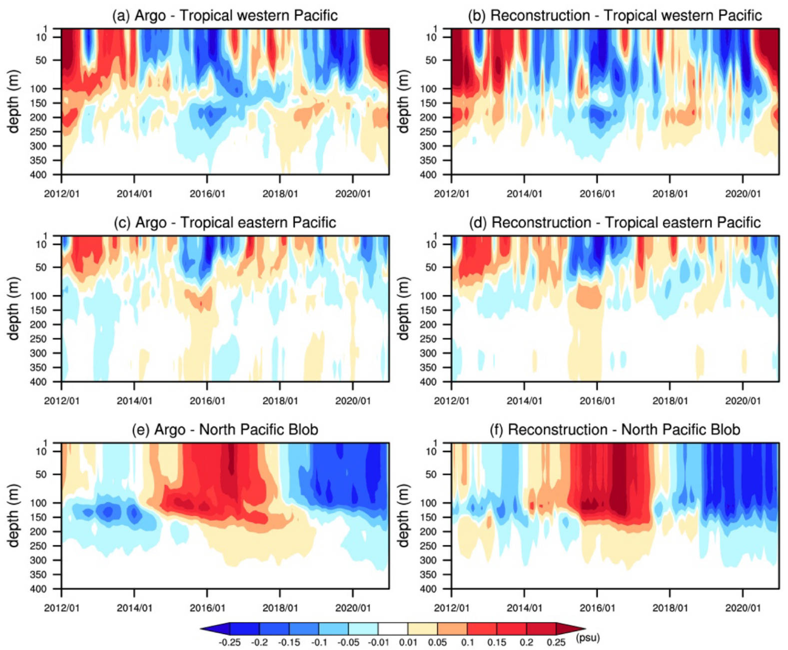

Figure 7. Comparisons of the Time-Depth Hovmöller plots for Argo in-situ (left column) and reconstructed (right column) ocean subsurface temperature anomalies over the three regions, including tropical western Pacific (a, b), tropical eastern Pacific (c, d) and North Pacific Blob (e, f), during 2012-2020.

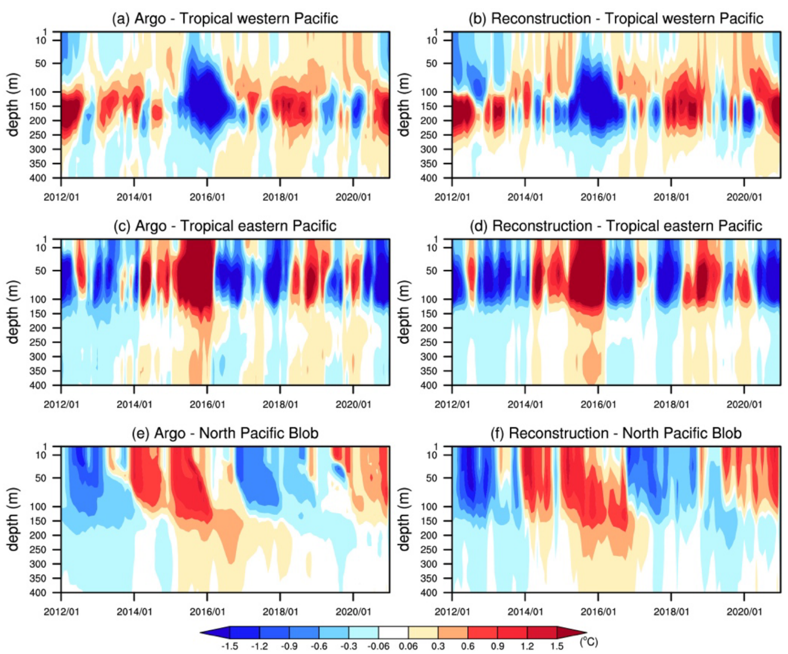

Figure 8. Same as Figure 7, but for salinity.

https://doi.org/10.5194/essd-2024-334
Preprint. Discussion started: 22 August 2024

To have a closer assessment, we also directly compare the time series for the Argo in-situ and the reconstructed temperature and salinity anomalies at various depths within the three regions (Fig. 9 and 10). The reconstructed temperature and salinity at various depths in both tropical western Pacific and the tropical eastern Pacific are generally consistent with Argo. Interestingly, there is some disagreement between the reconstructed and the Argo salinity anomalies in the tropical western Pacific at 120 m, even worse than 250 m, which may indicate the surface-subsurface decoupling around this depth. In general, there is less agreement between reconstruction and Argo in the North Pacific Blob region than the tropical Pacific, which may imply a stronger surface-subsurface coupling for the latter. Follow-up work is needed to understand the regional and vertical differences in the performance of the reconstruction algorithm.

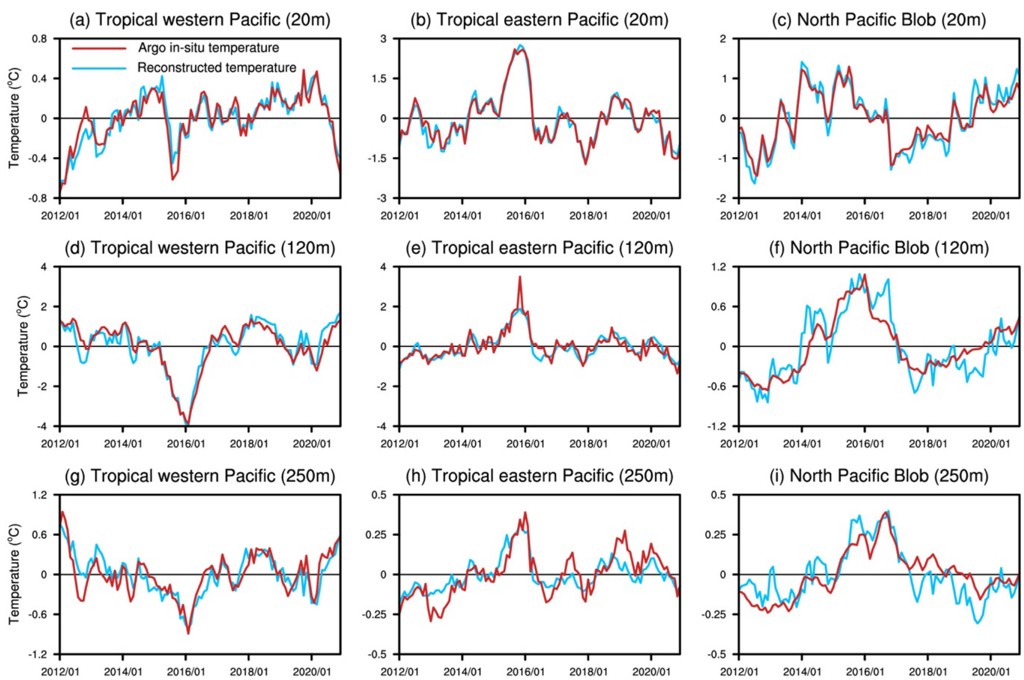

Figure 9. Comparisons of the time series of Argo in-situ (red line) and reconstructed (blue line) contrast time series for ocean subsurface monthly temperature anomalies at 20 m (a, b, c), 120 m (d, e, f) and 250 m (g, h, i) depths over these three regions during 2012-2020.

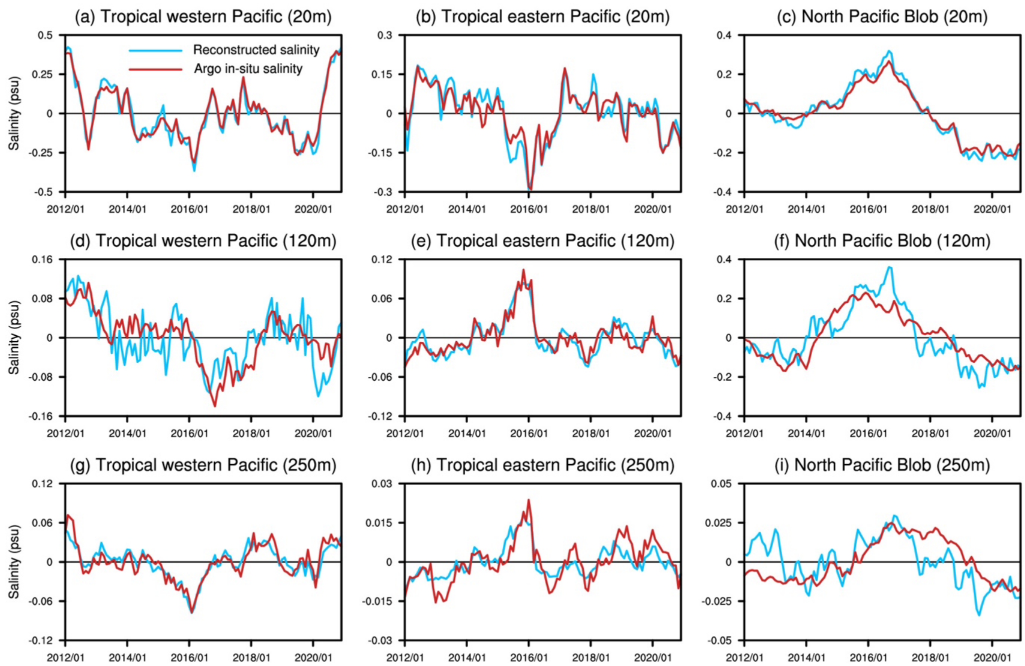

Figure 10. Same as Figure 9, but for salinity.

3.3 Overall assessment against the Argo dataset

A global assessment on the overall performance of our algorithm in space and time is provided. The spatial correlation coefficient between the Argo and the reconstructed fields (2°x2° ocean grids in total), as is done in Fig. 5c and f, is repeatedly computed for each month and for each vertical level (Fig. 11a and b). The highest correlations are found near the surface, as one would expect from the surface constraints being provided. Statistically significant correlations are found at all depths for both temperature and salinity ($p<10^{-5}$). Particularly high correlation coefficients are identified for 2015-16 as dominated by the large signals from the extreme El Niño. Similarly, but now at each ocean grid, the Argo-reconstruction correlation coefficient is computed for all months and all levels (Fig. 11c and d). Statistically significant correlations are identified for 99.9% global oceans excluding the ice-covered area ($p<10^{-5}$), implying that our algorithm can well capture both the vertical structure and the temporal evolution of temperature and salinity anomalies. The highest correlations are found over the tropical Pacific, the North Pacific, and the tropical Indian Ocean, which may suggest a strong surface-subsurface coupling over these regions, and the detailed mechanisms causing such spatial structure need further investigations. Meanwhile, this

https://doi.org/10.5194/essd-2024-334
Preprint. Discussion started: 22 August 2024

could also be attributed to the higher consistency between satellite and Argo data in tropical regions (Lee 2018).

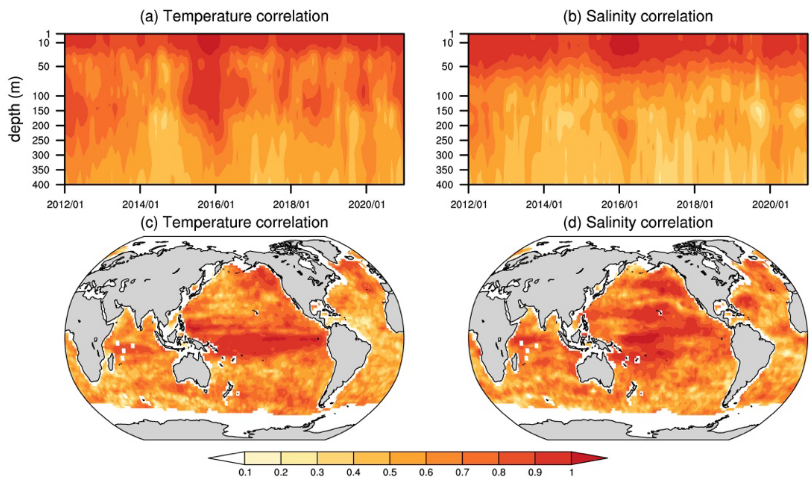

Figure 11. (a-d) Correlation coefficient between Argo in situ datasets and reconstructions (left column: temperature, right column: salinity) associated with the global map (top row) and depth (0-400 m with a 10 m interval)-time (from January 2012 to December 2020) Hovmöller for each grid point (bottom row). Both Argo in-situ and reconstructed datasets are interpolated to a 2° x 2° spatial resolution in this figure.

Figure 12 shows the root-mean-squared-error (RMSE) between the Argo and the reconstructed fields (2°x2° ocean grids in total). Unlike the correlation coefficient, the temperature and salinity reconstruction errors reach the largest at the depths of 50-100 meters and are smaller near the surface or below 200 m. The relatively small RMSE results from the strong agreement between satellite observations and Argo at the surface (Du and Zhang, 2015) and the weaker temperature and salinity variabilities in general below 200 m. In terms of spatial distribution, the RMSEs of temperature and salinity tend to be larger over the deep tropics, where it is warm and rainy, and over the Kuroshio and Gulf stream, where it is dominated by ocean fronts and storm tracks. Overall, the RMSE between the Argo and the reconstruction fields exhibits considerable variations in space and time, and is generally comparable on a global scale compared to some other machine learning-based algorithms (Tian et al., 2022).

https://doi.org/10.5194/essd-2024-334
Preprint. Discussion started: 22 August 2024

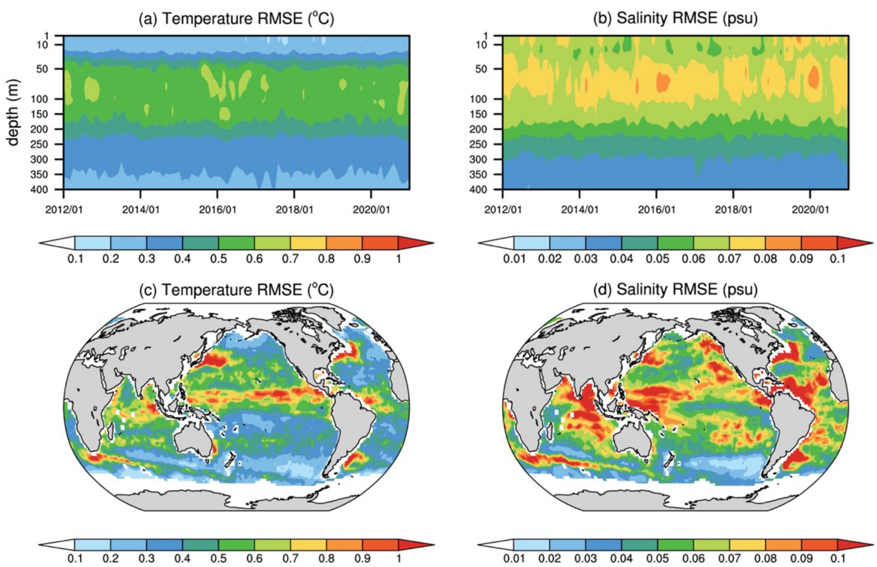

Figure 12. Same as Figure 11, but for the root-mean-squared-error (RMSE).

3.4 Evaluation against in-situ buoy measurements

Next, we regard the in-situ buoy measurements of subsurface temperature and salinity from TAO/ TRITON as true observations and compare them with our reconstruction together with other existing ocean subsurface datasets. We present the results for the site at 8° N, 137° E, where most temporally complete measurements are available in Fig. 13 for the purpose of illustration and show the results for another few sites that have reasonably long subsurface records in Fig. S3-S6 in Supplement. Overall, our reconstruction agrees well with the in-situ buoy measurements for both temperature and salinity and at various depths (Fig. 13), and it falls within the spread across other existing datasets. In some cases, our reconstruction clearly outperforms other subsurface datasets. For example, in early 2016, in-situ buoy measurements recorded a sharp increase in both temperature and salinity at 150 m. This feature is accurately captured by our reconstruction, but not by other products. A detailed inter-data comparison and investigations on the cause of data disagreement need to be done routinely in future studies.

https://doi.org/10.5194/essd-2024-334
Preprint. Discussion started: 22 August 2024

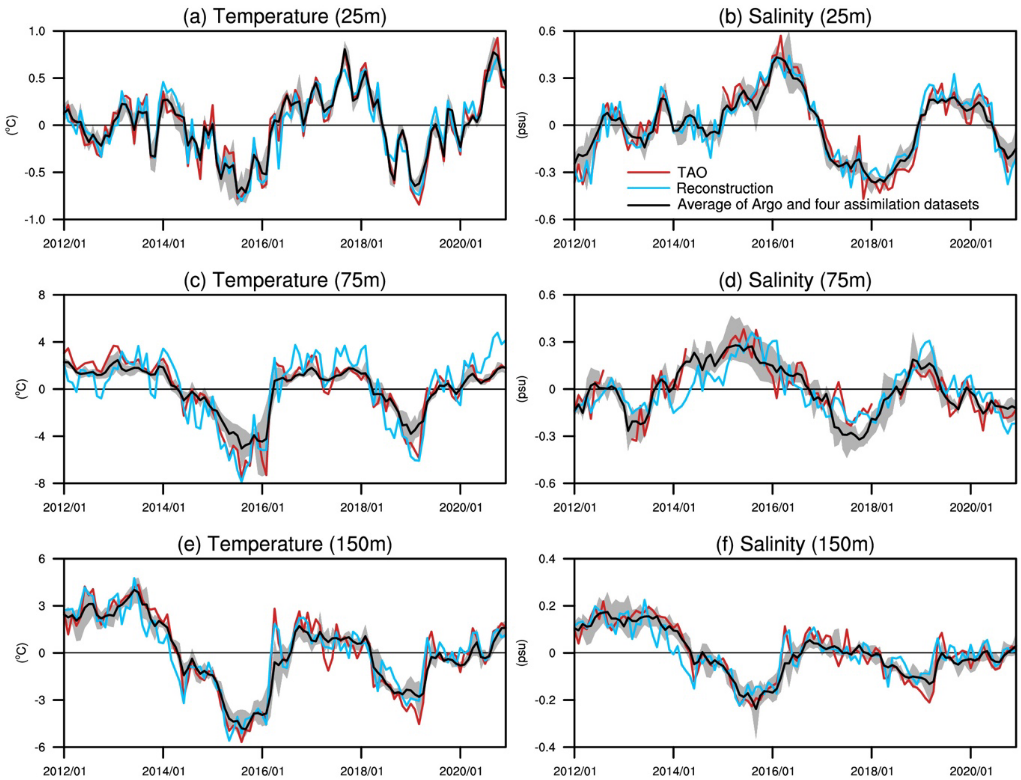

Figure 13. Comparisons between TAO/TRITON, our reconstruction, and other subsurface datasets at the site of 8° N, 137° E for the depths at 25 m (a, b), 75 m (c, d) and 150 m (e, f). The TAO/ TRITON time series is represented by the red curve, the reconstructed time series by the blue curve, and the average of Argo in-situ data and four assimilation data (ORAS5, SODA3, ECCO4r4, IAP) is depicted by the black curve. The gray shading curve denotes one standard deviation across the Argo, ORAS5, SODA3, ECCO4r4, and IAP datasets (see Data and Methods).

4 Discussion and outlook

In this study, our novel reconstruction algorithm provides a promising tool to develop a satellite-based dataset for ocean subsurface temperature and salinity that has a global coverage and a high spatial resolution. This algorithm achieves the reconstruction of subsurface ocean temperature and salinity anomalies solely based on surface data with satisfactory accuracy in comparison to actual observed values. Specifically, we first used CESM2 historical data to validate the accuracy of this algorithm as CESM2 model has self-consistent surface and subsurface variables. The reconstruction of CESM2 subsurface fields shows an impressive agreement in its spatial distribution, temporal variability, and long-term change compared to CESM2 actual values.

https://doi.org/10.5194/essd-2024-334
Preprint. Discussion started: 22 August 2024

After being verified by CESM2, we applied the algorithm to observations. The reconstructed temperature and salinity fields generally match those from the Argo in-situ observations in their large-scale patterns, vertical structures, and interannual variations. Interestingly, the algorithm yields satisfactory results even at deep subsurface levels (e.g., 200-400 m) where the signals are weak. Also, the reconstruction seems to be even better for salinity than for temperature. Furthermore, our reconstruction exhibits enhanced performance in the tropical oceans, and the reconstruction skill gradually diminishes with increasing depth as one would expect from the surface constraints of our algorithm. Finally, a comparison with temperature and salinity data from a TAO/TRITON site reveals that our reconstruction generally resides in the spread across major ocean assimilation or reanalysis products and can sometimes capture short-term and local variability that other products fail to capture. These results suggest that our reconstructed temperature and salinity fields can be readily used to complement the existing ocean subsurface products as an independent, satellite-based observational dataset. For example, we can use this dataset to assess the ocean heat content in various ocean regions. Besides, the usage of satellite observations presents a unique advantage of our reconstruction dataset that can achieve high spatio-temporal resolutions for studies on mesoscale ocean phenomena. To make such reconstructions possible, there is an urgent need to maintain continuous observations of satellite observations on ocean properties like SST, SSS, and SSH as emphasized here.

Limitations and challenges do exist for our proposed approach. Firstly, the reconstruction is less satisfactory in certain ocean regions, for example, the tropical Atlantic where ocean surface temperature and salinity barely covary (Kido et al., 2021). More generally, the potential error associated with our reconstruction can also come from other sources, including the imperfection of the algorithm (e.g., usage of 3 EOF modes) and the inherent errors of satellite datasets (Boutin et al., 2016; Yan et al., 2021). These challenges point to the need of improving the algorithm and minimizing the satellite observational error in future studies. Secondly, in comparison to machine learning methods, our approach falls short in reconstructing the deep ocean fields below 500 m (Tian et al., 2022). Nevertheless, our joint EOF-based algorithm is more interpretable as opposed to machine learning, allowing for a deeper understanding on the physics of temperature and salinity co-variability and the surface-subsurface coupling. Follow-up work along this line is currently underway. It is important to emphasize that in-situ measurements (e.g., Argo floats, CTD, moored buoys) remain necessary to provide independent subsurface observations, especially in the deep ocean.

Financial support

This research was supported by National Aeronautics and Space Administration Grant 80NSSC22K1025.

Author Contributions

S.H. conceived the original idea; S.L. performed the data analysis; S.L. and S.H. designed the research, interpreted the results, and wrote the manuscript.

Competing Interests

The authors declare no competing interests.

Data availability

Datasets produced by this study are available to the public at https://doi.org/10.5281/zenodo.13145129 (Liu, 2024).

The data used in the manuscript are publicly available for OISST (https://www.ncei.noaa.gov/products/optimum-interpolation-sst), OISSS (https://podaac.jpl.nasa.gov/dataset/OISSS_L4_multimission_7day_v1), SSH (https://podaac.jpl.nasa.gov/dataset/SEA_SURFACE_HEIGHT_ALT_GRIDS_L4_2SATS_5DAY_6THDEG_V_JPL2205), Argo in-situ dataset (https://www.seanoe.org/data/00412/52367/), ORAS5 (https://www.ecmwf.int/en/forecasts/dataset/ocean-reanalysis-system-5), SODA3 (https://www2.atmos.umd.edu/~ocean/index_files/soda3.15.2_mn_download_b.htm), ECCO4r4 (https://podaac.jpl.nasa.gov/dataset/ECCO_L4_OBP_05DEG_DAILY_V4R4), IAP (http://www.ocean.iap.ac.cn/pages/dataService/dataService.html?navAnchor=dataService), TAO/TRITON array (https://www.pmel.noaa.gov/tao/drupal/disdel/), CESM2 (https://esgf-node.llnl.gov/projects/cmip6/)

https://doi.org/10.5194/essd-2024-334
Preprint. Discussion started: 22 August 2024

References

Abraham, J. P., Baringer, M., Bindoff, N. L., Boyer, T., Cheng, L. J., Church, J. A., Conroy, J. L., Domingues, C. M., Fasullo, J. T., Gilson, J., Goni, G., Good, S. A., Gorman, J. M., Gouretski, V., Ishii, M., Johnson, G. C., Kizu, S., Lyman, J. M., Macdonald, A. M., Minkowycz, W. J., Moffitt, S. E., Palmer, M. D., Piola, A. R., Reseghetti, F., Schuckmann, K., Trenberth, K. E., Velicogna, I., Willis, J. K.: A review of global ocean temperature observations: Implications for ocean heat content estimates and climate change. Rev. Geophys., 51, 450-483. https://doi.org/10.1002/rog.20022, 2013.

Bagnell, A., and DeVries, T.: 20th century cooling of the deep ocean contributed to delayed acceleration of Earth's energy imbalance. Nat. Commun., 12, 4604. https://doi.org/10.1038/s41467-021-24472-3, 2021.

Boutin, J., Chao, Y., Asher, W. E., Delcroix, T., Drucker, R., Drushka, K., Kolodziejczyk, N., Lee, T., Reul, N., Reverdin, G., Schanze, J., Soloviev, A., Yu, L., Anderson, J., Brucker, L., Dinnat, E., Garcia, A. S., Jones, W. L., Maes, C., Meissner, T., Tang, W., Vinogradova, N., Ward, B.: Satellite and in situ salinity: Understanding near-surface stratification and subfootprint variability. Bull. Am. Meteorol. Soc., 97, 1391-1407. https://doi.org/10.1175/BAMS-D-15-00032.1, 2016.

Boutin, J., Reul, N., Köhler, J., Martin, A., Catany, R., Guimbard, S., Rouffi, F., Vergely, J. L., Arias, M., Chakroun, M., Corato, G., Estella-Perez, V., Hasson, A., Josey, S., Khvorostyanov, D., Kolodziejczyk, N., Mignot, J., Olivier, L., Reverdin, G., Stammer, D., Supply, A., Thouvenin-Masson, C., Turiel, A., Vialard, J., Cipollini, P., Donlon, C., Sabia, R., Mecklenburg, S.: Satellite-Based Sea Surface Salinity Designed for Ocean and Climate Studies. J. Geophys. Res. Oceans, 126, e2021JC017676. https://doi.org/10.1029/2021JC017676, 2021.

Carton, J. A., Chepurin, G. A., and Chen, L.: SODA3: A new ocean climate reanalysis. J. Clim., 31, 6967-6983. https://doi.org/10.1175/JCLI-D-18-0149.1, 2018.

Cheng, L., Trenberth, K. E., Fasullo, J., Boyer, T., Abraham, J., and Zhu, J.: Improved estimates of ocean heat content from 1960 to 2015. Sci. Adv., 3, e1601545. https://doi.org/10.1126/sciadv.1601545, 2017.

https://doi.org/10.5194/essd-2024-334
Preprint. Discussion started: 22 August 2024

Cullum, C., Rogers, K. H., Brierley, G., and Witkowski, E. T.: Ecological classification and mapping for landscape management and science: Foundations for the description of patterns and processes. Prog. Phys. Geogr., 40, 38-65. https://doi.org/10.1177/0309133315611573, 2016.

Danabasoglu, G., Lamarque, J.-F., Bacmeister, J., Bailey, D. A., DuVivier, A. K., Edwards, J., Emmons, L. K., Fasullo, J., Gar- cia, R., Gettelman, A., Hannay, C., Holland, M. M., Large, W. G., Lauritzen, P. H., Lawrence, D. M., Lenaerts, J. T. M., Lindsay, K., Lipscomb, W. H., Mills, M. J., Neale, R., Ole- son, K. W., Otto-Bliesner, B., Phillips, A. S., Sacks, W., Tilmes, S., van Kampenhout, L., Vertenstein, M., Bertini, A., Dennis, J., Deser, C., Fischer, C., Fox-Kemper, B., Kay, J. E., Kinni- son, D., Kushner, P. J., Larson, V. E., Long, M. C., Mickel- son, S., Moore, J. K., Nienhouse, E., Polvani, L., Rasch, P. J., and Strand, W. G.: The Community Earth System Model Version 2 (CESM2), J. Adv. Model. Earth Sy., 12, e2019MS001916, https://doi.org/10.1029/2019MS001916, 2020.

Du, Y., and Zhang, Y.: Satellite and Argo observed surface salinity variations in the tropical Indian Ocean and their association with the Indian Ocean dipole mode. J. Clim., 28, 695-713. https://doi.org/10.1175/JCLI-D-14-00435.1, 2015.

ECCO Consortium, Fukumori, I., Wang, O., Fenty, I., Forget, G., Heimbach, P., and Ponte, R. M.: Synopsis of the ECCO Central Production Global Ocean and Sea- Ice State Estimate (Version 4 Release 4). https://doi.org/10.5281/zenodo.4533349, 2021.

Fournier, S., and Lee, T.: Seasonal and interannual variability of sea surface salinity near major river mouths of the world ocean inferred from gridded satellite and in-situ salinity products. Remote Sens., 13, 728. https://doi.org/10.3390/rs13040728, 2021.

Fournier, S., Willis, J., Killett, E., Qu, Z., and Zlotnicki, V.: JPL MEaSUREs Gridded Sea Surface Height Anomalies Version 2205. https://doi.org/10.5067/SLREF-CDRV3, 2022.

Fujii, Y., and Kamachi, M.: Three-dimensional analysis of temperature and salinity in the equatorial Pacific using a variational method with vertical coupled temperature-salinity empirical orthogonal function modes. J. Geophys. Res. Oceans, 108. https://doi.org/10.1029/2002JC001745, 2003.

https://doi.org/10.5194/essd-2024-334
Preprint. Discussion started: 22 August 2024

Gaillard, F., Reynaud, T., Thierry, V., Kolodziejczyk, N., and von Schuckmann, K.: In situ–based reanalysis of the global ocean temperature and salinity with ISAS: Variability of the heat content and steric height. J. Clim., 29, 1305-1323. https://doi.org/10.1175/JCLI-D-15-0028.1, 2016.

Guinehut, S., Dhomps, A. L., Larnicol, G., and Le Traon, P. Y.: High resolution 3-D temperature and salinity fields derived from in situ and satellite observations. Ocean Sci., 8, 845-857. https://doi.org/10.5194/os-8-845-2012, 2012.

Hayes, S. P., Mangum, L. J., Picaut, J., Sumi, A., and Takeuchi, K.: TOGA-TAO: A moored array for real-time measurements in the tropical Pacific Ocean. Bull. Am. Meteorol. Soc., 72, 339-347. https://doi.org/10.1175/1520- 0477(1991)072%3C0339:TTAMAF%3E2.0.CO;2, 1991.

Hosoda, S., Ohira, T., and Nakamura, T.: A monthly mean dataset of global oceanic temperature and salinity derived from Argo float observations. JAMSTEC Rep. Res. Dev., 8, 47-59. https://doi.org/10.5918/jamstecr.8.47, 2008.

Huang, B., Liu, C., Freeman, E., Graham, G., Smith, T., and Zhang, H. M.: Assessment and intercomparison of NOAA daily optimum interpolation sea surface temperature (DOISST) version 2.1. J. Clim., 34, 7421-7441. https://doi.org/10.1175/JCLI-D-21-0001.1, 2021.

Hughes, T. P., Baird, A. H., Bellwood, D. R., Card, M., Connolly, S. R., Folke, C., Grosberg, R., Hoegh-Guldberg, O., Jackson, J. B., Kleypas, J., Lough, J. M., Marshall, P., Nyström, M., Palumbi, S. R., Pandolf, J. M., Rosen, B., Roughgarden, J.: Climate change, human impacts, and the resilience of coral reefs. Science, 301, 929-933. https://doi.org/10.1126/science.1085046, 2003.

Kido, S., Nonaka, M., and Tanimoto, Y.: Sea surface temperature–salinity covariability and its scale-dependent characteristics. Geophys. Res. Lett., 48, e2021GL096010. https://doi.org/10.1029/2021GL096010, 2021.

Lee, T.: Consistency of Aquarius sea surface salinity with Argo products on various spatial and temporal scales. Geophys. Res. Lett., 43, 3857-3864. https://doi.org/10.1002/2016GL068822, 2016.

Liang, X., Liu, C., Ponte, R. M., and Chambers, D. P.: A comparison of the variability and changes in global ocean heat content from multiple objective analysis products during the Argo period. J. Clim., 34, 7875-7895. https://doi.org/10.1175/JCLI-D-20-0794.1, 2021.

Liu, C., Liang, X., Ponte, R., and Chambers, D.: Global ocean salinity measurements have some serious issues after 2015. Preprint. Retrieved from https://assets.researchsquare.com/files/rs-1836193/v1_covered.pdf?c=1657561560, 2022.

Liu, S.: Reconstructing Ocean Subsurface Temperature and Salinity with Satellite Observations [Data set]. Zenodo. https://doi.org/10.5281/zenodo.13145129, 2024.

Loew, A., Bell, W., Brocca, L., Bulgin, C. E., Burdanowitz, J., Calbet, X., Donner, R. V., Ghent, D., Gruber, A., Kaminski, T., Kinzel, J., Klepp, C., Lambert, J. C., Schaepman-Strub, G., Schröder, M., Verhoelst, T.: Validation practices for satellite-based Earth observation data across communities. Rev. Geophys., 55, 779-817. https://doi.org/10.1002/2017RG000562, 2017.

Maes, C.: A note on the vertical scales of temperature and salinity and their signature in dynamic height in the western Pacific Ocean: Implications for data assimilation. J. Geophys. Res. Oceans, 104, 11037-11048. https://doi.org/10.1029/1999JC900032, 1999.

Maes, C., and Behringer, D.: Using satellite-derived sea level and temperature profiles for determining the salinity variability: A new approach. J. Geophys. Res. Oceans, 105, 8537-8547. https://doi.org/10.1029/1999JC900279, 2000.

Manucharyan, G., Siegelman, L., and Klein, P.: Estimation of surface and deep flows from sparse SSH observations of geostrophic ocean turbulence using Deep Learning. https://doi.org/10.31223/osf.io/m8f3x, 2019.

Melnichenko, O., Hacker, P., Potemra, J., Meissner, T., and Wentz, F.: Aquarius/SMAP sea surface salinity optimum interpolation analysis. IPRC Technical Note. (No. 7, May 7, 2021). https://doi.org/10.5067/smp10-4u7cs, 2021.

Meng, L., Yan, C., Zhuang, W., Zhang, W., and Yan, X. H.: Reconstruction of three- dimensional temperature and salinity fields from satellite observations. J. Geophys. Res. Oceans, 126, e2021JC017605. https://doi.org/10.1029/2021JC017605, 2021.

Ponte, R. M., Sun, Q., Liu, C., and Liang, X.: How salty is the global ocean: weighing it all or tasting it a sip at a time? Geophys. Res. Lett., 48, e2021GL092935. https://doi.org/10.1029/2021GL092935, 2021.

Riser, S. C., Freeland, H. J., Roemmich, D., Wijffels, S., Troisi, A., Belbéoch, M., Gilbert, D., Xu, J., Pouliquen, S., Thresher, A., Le Traon, P.-Y., Maze, G., Klein, B., Ravichandran, M., Grant, F.,

https://doi.org/10.5194/essd-2024-334
Preprint. Discussion started: 22 August 2024

Poulain, P.-M., Suga, T., Lim, B., Sterl, A., Sutton, P., Mork, K.-A., Velez-Belchi, P. J., Ansorge, I., King, B., Turton, J., Baringer, M., Jayne, S. R.: Fifteen years of ocean observations with the global Argo array. Nat. Clim. Change, 6, 145-153. https://doi.org/10.1038/nclimate2872, 2016.

Roemmich, D., Alford, M. H., Claustre, H., Johnson, K., King, B., Moum, J., Oke, P., Owens, W. B., Pouliquen, S., Purkey, S., Scanderbeg, M., Suga, T., Wijffels, S., Zilberman, N., Bakker, D., Baringer, M., Belbeoch, M., Bittig, H.C., Boss, E., Calil, P., Carse, F., Carval, T., Chai, F., Conchubhair, D.Ó., d'Ortenzio, F., Dall'Olmo, G., Desbruyeres, D., Fennel, K., Fer, I., Ferrari, R., Forget, G., Freeland, H., Fujiki, T., Gehlen, M., Greenan, B., Hallberg, R., Hibiya, T., Hosoda, S., Jayne, S., Jochum, M., Johnson, G. C., Kang, K., Kolodziejczyk, N., Körtzinger, A., Le Traon, P.-Y., Lenn, Y.-D., Maze, G., Mork, K. A., Morris, T., Nagai, T., Nash, J., Naveira Garabato, A., Olsen, A., Pattabhi, R. R., Prakash, S., Riser, S., Schmechtig, C., Schmid, C., Shroyer, E., Sterl, A., Sutton, P., Talley, L., Tanhua, T., Thierry, V., Thomalla, S., Toole, J., Troisi, A., Trull, T. W., Turton, J., Velez-Belchi, P. J., Walczowski, W., Wang, H., Wanninkhof, R., Waterhouse, A. F., Waterman, S., Watson, A., Wilson, C., Wong, A. P. S., Xu, J., and Yasuda, I.: On the Future of Argo: A Global, Full-Depth, Multi-Disciplinary Array, Front. Mar. Sci., 6, 439, https://doi.org/10.3389/fmars.2019.00439, 2019.

Skliris, N., Marsh, R., Josey, S. A., Good, S. A., Liu, C., and Allan, R. P.: Salinity changes in the World Ocean since 1950 in relation to changing surface freshwater fluxes. Clim. Dynam., 43, 709-736. https://doi.org/10.1007/s00382-014-2131-7, 2014.

Stendardo, I., Rhein, M., and Hollmann, R.: A high resolution salinity time series 1993– 2012 in the North Atlantic from Argo and Altimeter data. J. Geophys. Res. Oceans, 121, 2523-2551.https://doi.org/10.1002/2015JC011439, 2016.

Stommel, H.: Note on the use of the TS correlation for dynamic height anomaly computations. J. Mar. Res., 6, 85–92. https://elischolar.library.yale.edu/journal_of_marine_research/627, 1947.

Tang, B., Zhao, D., Cui, C., and Zhao, X.: Reconstruction of ocean temperature and salinity profiles in the Northern South China Sea using satellite observations. Front. Mar. Sci., 9, 945835. https://doi.org/10.3389/fmars.2022.945835, 2022.

Tian, T., Cheng, L., Wang, G., Abraham, J., Wei, W., Ren, S., Zhu, J., Song, J., Leng, H.: Reconstructing ocean subsurface salinity at high resolution using a machine learning approach. Earth Syst. Sci. Data, 14, 5037-5060. https://doi.org/10.5194/essd-14-5037-2022, 2022.

Troccoli, A., and Haines, K.: Use of the temperature–salinity relation in a data assimilation context. J. Atmos. Oceanic Technol., 16, 2011-2025. https://doi.org/10.1175/1520-0426(1999)016%3C2011:UOTTSR%3E2.0.CO;2, 1999.

Vinogradova, N., Lee, T., Boutin, J., Drushka, K., Fournier, S., Sabia, R., Stammer, D., Bayler, E., Reul, N., Gordon, A., Melnichenko, O., Li, L., Hackert, E., Martin, M., Kolodziejczyk, N., Hasson, A., Brown, S., Misra, S., Lindstrom, E.: Satellite salinity observing system: Recent discoveries and the way forward. Front. Mar. Sci., 6, 428925. https://doi.org/10.3389/fmars.2019.00243, 2019.

Wang, H., Wang, G., Chen, D., and Zhang, R.: Reconstruction of three-dimensional Pacific temperature with Argo and satellite observations. Atmos-Ocean, 50, 116-128. https://doi.org/10.1080/07055900.2012.742421, 2012.

Wong, A. P., Gilson, J., and Cabanes, C.: Argo salinity: bias and uncertainty evaluation. Earth Syst. Sci. Data, 15, 383–393. https://doi.org/10.5194/essd-15-383-2023, 2023.

Wong, A. P. S., Wijffels, S. E., Riser, S. C., Pouliquen, S., Hosoda, S., Roemmich, D., Gilson, J., Johnson, G. C., Martini, K., Murphy, D. J., Scanderbeg, M., Bhaskar, T. V. S. U., Buck, J. J. H., Merceur, F., Carval, T., Maze, G., Cabanes, C., André, X., Poffa, N., Yashayaev, I., Barker, P. M., Guinehut, S., Belbéoch, M., Ignaszewski, M., Baringer, M. O'N., Schmid, C., Lyman, J. M., McTaggart, K. E., Purkey, S. G., Zilberman, N., Alkire, M. B., Swift, D., Owens, W. B., Jayne, S. R., Hersh, C., Rob bins, P., West-Mack D., Bahr, F., Yoshida, S., Sutton, P. J. H., Cancouët, R., Coatanoan, C., Dobbler, D., Juan, A. G., Gourrion, J., Kolodziejczyk, N., Bernard, V., Bourlès, B., Claustre, H., D'Ortenzio, F., Le Reste, S., Le Traon, P.-Y., Rannou, J.-P., Saout-Grit, C., Speich, S., Thierry, V., Verbrugge, N., Angel- Benavides, I. M., Klein, B., Notarstefano, G., Poulain, P.-M., Vélez-Belchí, P., Suga, T., Ando, K., Iwasaska, N., Kobayashi, T., Masuda, S., Oka, E., Sato, K., Nakamura, T., Sato, K., Takatsuki, Y., Yoshida, T., Cowley, R., Lovell, J. L., Oke, P. R., van Wijk, E. M., Carse, F., Donnelly, M., Gould, W. J., Gowers, K., King, B. A., Loch, S. G., Mowat, M., Turton, J., Rama, R. E. P., Ravichandran M., Freeland, H. J., Gaboury, I., Gilbert, D., Greenan, B. J. W., Ouellet, M., Ross, T., Tran, A., Dong, M., Liu, Z., Xu, J., Kang, K., Jo, H. J., Kim, S.-D., and Park, H.-M.: Argo Data 1999–2019: Two Million Temperature- Salinity Profiles and

https://doi.org/10.5194/essd-2024-334
Preprint. Discussion started: 22 August 2024

Subsurface Velocity Observations from a Global Array of Profiling Floats, Front. Mar. Sci., 7, 700, https://doi.org/10.3389/fmars.2020.00700, 2020.

Wunsch, C.: Modern observational physical oceanography: understanding the global ocean. Princeton University Press., 2015.

Yan, H., Wang, H., Zhang, R., Bao, S., Chen, J., and Wang, G.: The inconsistent pairs between in situ observations of near surface salinity and multiple remotely sensed salinity data. Earth Space Sci., 8, e2020EA001355. https://doi.org/10.1029/2020EA001355, 2021.

Zhang, J., Zhang, X., Wang, X., Ning, P., and Zhang, A.: Reconstructing 3D ocean subsurface salinity (OSS) from T–S mapping via a data-driven deep learning model. Ocean Model., 184, 102232. https://doi.org/10.1016/j.ocemod.2023.102232, 2023.

Zhou, G., Han, G., Li, W., Wang, X., Wu, X., Cao, L., and Li, C.: High-Resolution Gridded Temperature and Salinity Fields From Argo Floats Based on a Spatiotemporal Four- Dimensional Multigrid Analysis Method. J. Geophys. Res. Oceans, 128, e2022JC019386. https://doi.org/10.1029/2022JC019386, 2023.

Zuo, H., Balmaseda, M. A., Tietsche, S., Mogensen, K., and Mayer, M.: The ECMWF operational ensemble reanalysis–analysis system for ocean and sea ice: a description of the system and assessment. Ocean Sci., 15, 779-808. https://doi.org/10.5194/os-15-779-2019, 2019.